A Granular Model of Equiaxed Mushy Zones: Formation of a Coherent Solid and Localization of Feeding.

Stéphane Vernède[1,2], Philippe Jarry[2], Michel Rappaz[1]

Published in Acta Materialia, Volume 54, Issue 15, September 2006, Pages 4023-4034
view at publisher

[1] Computational Materials Laboratory,
Ecole Polytechnique Fédérale de Lausanne,
Station 12, Lausanne, CH-1015 Switzerland

[2]Alcan-CRV,
ZI Centr'alp, 0725 rue Aristide Berges,
BP 27, Voreppe, FR-38341 France

keywords: solidification, modeling, percolation, liquid infiltration, hot tearing

Abstract

The gradual transformation of a mushy zone during alloy solidification, from a continuous liquid film network to a fully coherent solid, has been simulated using a granular model. Based on a Voronoi tessellation of a random set of nucleation centers, solidification within each polyhedron is computed considering back-diffusion and coalescence. In the network of connected liquid films, a pressure drop calculation is performed assuming a Poiseuille flow in each channel, Kirchhoff's conservation of flow at nodal points and flow Losses compensating solidification shrinkage (KPL model). In addition to intergranular liquid pressure maps, the model shows the progressive formation of grains clusters, the localisation of the flow at very high solid fraction, and thus natural transitions of the mushy zone.

1 Introduction

Hot tearing is a spontaneous failure of a metal during its solidification and remains one of the most severe defects in casting and welding processes. Hot tear surfaces reveal an intergranular profile exhibiting a smooth surface with a few small spikes ($\sim 10\mu$m)

resulting from local plastic deformation of solid bridges or solidification of last liquid menisci [1].

During solidification, thermal strains impose significant deformations to the partially coherent solid. In regions of a casting where the mushy solid globally contracts, this can compensate solidification shrinkage. However, in regions where it is under global expansion, the dilatation of the mushy solid adds to solidification shrinkage and may induce hot cracks if liquid feeding is insufficient. This will be localised in regions where the mushy zone is most vulnerable to tensile strains, i.e., at grain boundaries.

Borland already pointed out that hot tears should occur in regions of the mushy zone where its permeability is very low (i.e., difficulty of feeding), but where bridging between the solid grains has not yet occurred to a large extent (i.e., brittle continuous liquid films still present at grain boundaries) [2]. Considering such arguments, Clyne and Davies developed a hot tearing criterion based on the solidification time spent in this vulnerable zone called interdendritic separation or brittle temperature range [3]. The limits of this zone were stated to be for solid fraction g_s between 0.9 and 0.99: below 0.9, feeding is still possible, above 0.99, the solid is fully coherent and ductile. Yet, solid fractions at which these transitions occur remain ill defined.

Another approach introduced by Feurer computes the liquid flow in the mush and the associated pressure drop induced by solidification shrinkage [4]. The first two-phase approach, accounting also for the deformation of the solid phase, was derived by Rappaz et al. [5]. In the so-called RDG criterion, a hot tear is considered to nucleate if the pressure deep in the mush is lower than a prescribed cavitation pressure. Following a similar line, Braccini et al. [6] extended the RDG criterion to the propagation of a hot tear. Using advanced rheological models for the deformation of a mushy solid [7], M'Hamdi et al. [8] and then Mathier et al. [9] developed a more rigorous two-phase formalism, but similar in essence to the RDG criterion, of hot tearing formation.

One of the main limitations of all these average methods is their inability to account for the localisation of strains (and hot tears) at grain/cluster boundaries. The fundamental reason for this localisation is that liquid films remain (or solid bridging occurs) at lower temperature at grain boundaries as compared with intragranular regions. Bridging or coalescence of dendrites or grains has been studied recently by Rappaz et al. [10]. Before reaching a fully coherent solid in which all the grains are linked by solid bridges (or by some eutectics), another transition of the mushy zone occurs when solid grains become sufficiently interlocked to transmit significant stresses in both shearing and traction [7, 11]. These two transitions are central for two-phase approaches, as they define points where the mechanical properties of the mushy zone drastically change. Yet, once again, solid fractions at which they occur remain ill defined.

In order to study the gradual formation of a coherent solid phase in globular alloys, an original approach has been proposed by Mathier et al. [12]. In this model, grains are approximated by polyhedrons based on the Voronoi diagram of a random set of

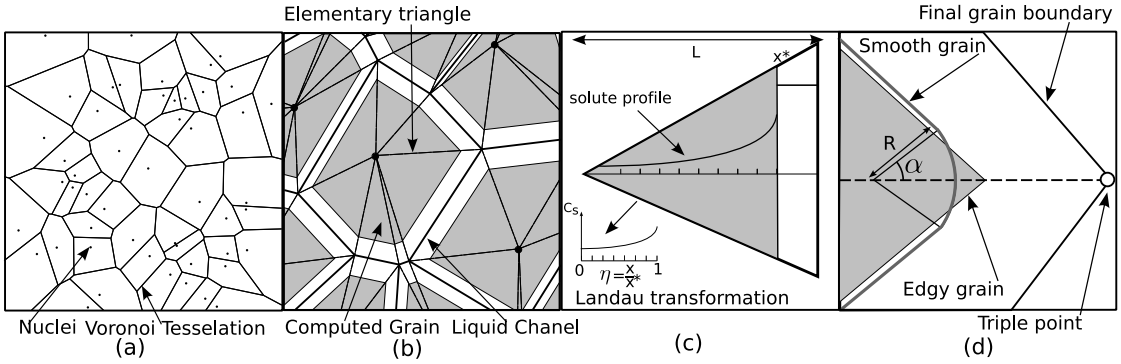

Figure 1: Various enlargements of the granular model: Voronoi tessellation associated with the nuclei centres (a); shape of the grains during solidification (b); solute balance within one triangle (c); smoothing procedure of the solid-liquid interface near the grain corners (d).

nuclei. Solidification of each grain can be computed using a microsegregation model, which includes a coalescence contribution near the end of solidification. Vernède et al. further simplified the assumptions of this model, in order to compute the solidification of large and non-isothermal mushy zones. Then, they coupled this solidification model with an intergranular feeding calculation [13].

Granular models have already been introduced to describe the ductility [14] or liquid feeding [15] of mushy zones, but they all rely on a regular arrangement of grains. As for the work of Mathier et al. and Vernède et al. [12, 13], the present contribution considers a random network of grains for the calculation of solidification and feeding in a gobular mushy zone. It goes beyond the latest work of Vernède et al. in several ways: i) the solidification model has been modified to account for rounded instead of polygonal grains; ii) the gradual formation of a coherent solid is analysed based on percolation theory; iii) the localisation of feeding at high volume fraction of solid is shown to naturally appear in a stochastic arrangement of grains; iv) the various transitions of the mushy zone morphology are defined with respect to the equilibrium phase diagram.

In a first part, we briefly present the granular model of solidification and liquid feeding, outlining the improvements made with respect to our previous model [13]. In the following section, localisation of feeding and cluster formation during solidification are shown and analysed. Finally, the last section presents morphological maps of the mushy zone based on the various transitions calculated with the model.

2 Granular model of a mushy zone

2.1 Solidification model

The 2-dimensional (2D) solidification model has been developed initially by Mathier and Rappaz [12] and was further improved by Vernède and Rappaz [13]. It will only be briefly

summarised here. The model assumes random nucleation centres in a plane with a given density, random orientation and simultaneous nucleation of the grains. Further assuming that the temperature difference across the average grain size is small with respect to the undercooling (i.e., small thermal gradient), the final grain structure should be close to the Voronoi tessellation of the set of nuclei (Fig. 1, (a)) [16]. In the present work, the Voronoi tessellation was computed using the free access software *qhull* [17].

In order to further simplify the solidification model, the smooth interface of each grain during growth is approximated by a linear segment in each triangle connecting the nucleation centre with a Voronoi segment. By construction, these segments are perpendicular to the vectors connecting the nucleation centres, and the two triangles issued from the same Voronoi segment are symmetrical, (Fig. 1, (b)).

Neglecting the solute flux between elementary triangles, solidification is reduced to a monodimensional problem in each triangle. The temperature of the system is imposed, either uniform or given by a fixed thermal gradient and decreasing with a given cooling rate. Complete diffusion is assumed in the liquid, while back-diffusion in the solid is calculated according to a Landau transformation, i.e., transformation of the solid domain [0,x*(t)], where x* is the position of the interface, into the reference 1D domain [0,1]. The model is therefore similar to that of Ohnaka [18].(Fig. 1, (c)).

This model leads to polyhedral grains (edgy grains model) [12][13], yet surface tension should tend to remelt the edgy corners. In order to make the grains smoother, a simple model which accounts for this effect has been derived (Fig. 1, (d))[19]. The position of the linear segments being known at a given time from the 1D microsegregation model, the edges are made round with an arc of a circle, the radius of which being evaluated from a solute flux balance. This flux is induced by the difference of solute concentrations between the curved and flat interfaces (Gibbs-Thomson effect). The radius of curvature, R, at a given corner is approximated to:

$$R = f(\alpha) \left(\frac{D_l \Gamma_{sl}}{|\dot{T}|} \right)^{1/3} \tag{1}$$

where Γ_{sl} is the Gibbs-Thomson coefficient for the solid liquid interface, D_l is the solute diffusion coefficient in the liquid phase, $\dot{T}$ is the cooling rate, $f(\alpha)$ is a given dimensionless function of the angle α of the considered edgy tip of the grain. Note that both the finite diffusion in the liquid and the Gibbs-Thomson effect were neglected for the determination of the flat interfaces position, while they have to be considered for the estimation of R.

The procedure of rounding the grain interfaces does not change the topological transitions of the mushy zone (built-up of a coherent network, disappearance of the continuous liquid films), but it changes the volume fractions of solid at which they occur. Indeed, as the interfaces are now rounded near triple points, the liquid pockets increase the liquid fraction. In order to keep a constant solid fraction (Fig. 1, (d)), the flat parts of the

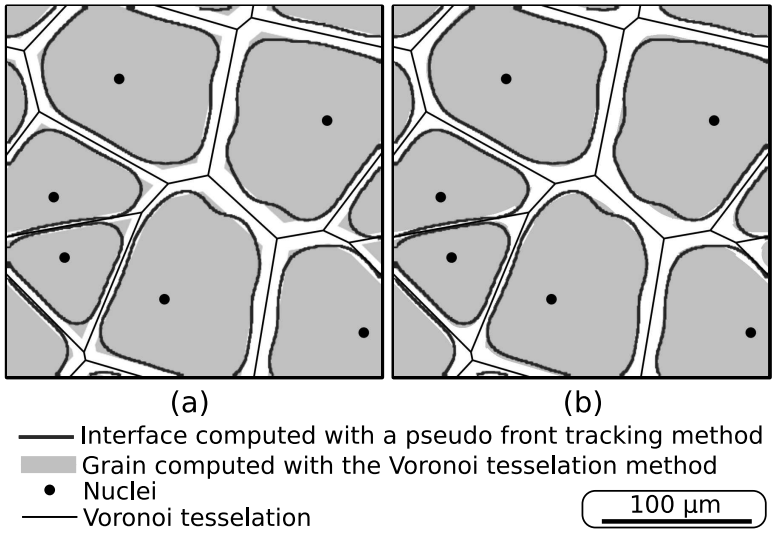

Figure 2: Grain shapes for an Al-1wt%Cu alloy cooled down at -1 K/s for $g_s = 0.75$ and a average grain density of $10^8 m^{-2}$ (average final grain size of 100 μm). The grains outlined in grey corresponds to the present polyhedral (a) and round (b) grain model. The shape can be compared with that calculated with a pseudo front tracking method [20].

interface are moved slightly forward. Further details on this solidification model with curved triple points are given in [19].

Figure 2 shows a comparison between the results of the present model for both polyhedral and smooth grain interfaces and those obtained with a pseudo front tracking (PFT) method.[20] The PFT method, which is close to a level set method, allows to track an interface while calculating solute diffusion and curvature. As for the phase field technique, it requires a fine mesh to give accurate results which, otherwise, do not depend on any approximation. As can be seen in Fig. 2 (b) for the smooth granular model, the predicted grain shapes are close to those obtained with the PFT method, while the sharp edge model predicts fairly well the position of the flat interfaces but clearly gives wrong results near the grain corners (Fig. 2 (a)). Note that, as the solidification model considers individual triangles of the Voronoi tessellation, the interfaces are not necessarily continuous at the grains corners, as already pointed out by Mathier et al.[12]. However, these few discontinuities are not affecting much the topological transformations of the mushy zone, the fraction of solid at which they occur or the intergranular feeding.

When two flat interfaces get very close to each other, the coalescence undercooling introduced by Rappaz et al. [10] is considered in the calculations, in a way similar to [12][13]. This undercooling, which is a function of the grain boundary energy, is calculated for each boundary IJ of the Voronoi tessellation, assuming a simplified Read-Shockley distribution, i.e., $\gamma_{gb,IJ}$ varies linearly from 0 to $\gamma_{gb,max}$ for $(|\theta_I - \theta_J|)$ varying from 0° to 20° and is fixed to $\gamma_{gb,max}$ above. θ_I and θ_J are the two orientation angles of grains I and J, respectively ($0 < |\theta_I - \theta_J| < 45$ deg. for a cubic symmetry) and $\gamma_{gb,max}$ is the surface energy of the disordered boundary. As coalescence effects are felt when the liquid

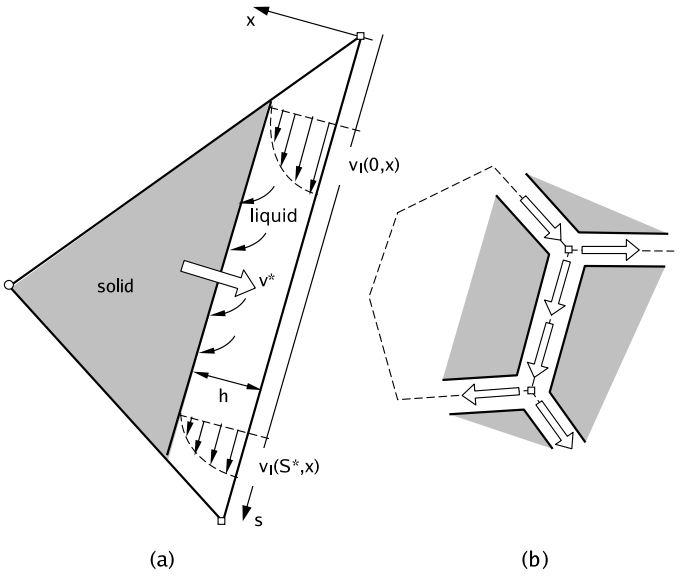

Figure 3: Fluid flow within a channel (a) and connectivity of these channels at triple points (b).

film thickness is of the order of the diffuse solid-liquid interface thickness ($\delta \sim 1-3$ nm), the solidification model of Mathier et al.[12] has been simplified as follows in order to speed up the computations. When the two solid-liquid interfaces are closer than δ, the exact position of the interface is no longer computed. Back diffusion in the solid fixes the concentration of the thin remaining liquid film and when the liquid composition reaches the coalescence line (for the prescribed temperature), the grain boundary is considered to be dry or solid. When the liquid film thickness is of the order of δ, the permeability of the liquid channel (see next section) is very low and the depression required to nucleate a void in this channel is very large (on the order of GPa). Therefore, this channel is equivalent to a *mechanical contact* for both feeding and mechanical resistance aspects. Hereafter when a grain boundary is dry or the liquid film is smaller than δ this status will be called mechanical contact.

2.2 Liquid feeding model

Since the densities of the solid, ρ_s, and the liquid, ρ_l, are not equal, solidification induces shrinkage. In a first step, it is assumed that the solid remains fixed and that no pore forms. This means that solidification shrinkage should be fully compensated by liquid flow. The speed of the liquid at a solid liquid interface is then given by :

$$v_{l,n} = -\beta v^* \tag{2}$$

where β is the solidification shrinkage ($\beta = (\frac{\rho_s}{\rho_l}) - 1$), and v^* is the speed of the (flat) solid-liquid interface. The normal $\mathbf{n}$ to the interface along which $\mathbf{v}_l$ is projected is pointing toward the liquid. Integration of the mass conservation for an incompressible flow

($\mathbf{div}(v_l) = 0$) over the width of a channel leads to [13]:

$$\frac{\partial I(s)}{\partial s} = -2\beta v^* \tag{3}$$

where s is the coordinate along the length of the channel (Fig. 3) and I is the liquid flow. Assuming a Poiseuille flow at any location in the channel, the flux I is directly linked with the pressure gradient:

$$I(s) = -\frac{2h^3}{3\mu}\frac{\partial P}{\partial s} \tag{4}$$

where μ is the viscosity of the fluid and h the liquid channel half width. Equations (3) and (4) give the master equation:

$$\frac{\partial^2 P}{\partial s^2} = \frac{3\mu}{h^3}\beta v^* \tag{5}$$

Finally, a Kirchoff condition ensures conservation of the flux at each node, j:

$$\forall j \quad \sum_i I_{i\to j} = 0 \tag{6}$$

where $I_{i\to j}$ is the fluid flux at node j coming from its neighbor i. As the relation between pressure drop and fluid flow is locally linear, the network of liquid channels is equivalent to an electrical resistance network. However, this network has flow losses corresponding to the shrinkage term, i.e., the resistances are not well insulated from the board on which they are fixed.

The justification of using a Poiseuille flow approximation, which supposes a no-slip condition at the boundaries, whereas a flow normal to the solid-liquid boundary is compensating shrinkage is given in [13]. A weak formulation of equations (5) and (6) can be obtained with standard monodimensional test functions $\phi_{i\to k}(s)$ which, for a channel in between nodes i and k, have the value 1 at the coordinate $s = s_i$, 0 at $s = s_k$, and is linear in between. One has:

$$\int_\Omega \frac{2h^3}{3\mu}\frac{\partial^2 P}{\partial s^2}\phi_{i\to k} ds = \int_\Omega 2\beta v^* \phi_{i\to k} ds \tag{7}$$

where Ω is the Voronoi tessellation of the set of nuclei. Integrating by part the first term and developing the pressure field as a summation over the test functions $\phi_{i\to k}$ (Galerkin formulation), equation 7 can be discretised on each node, thus giving for a node i :

$$\sum_{k \in \text{ neighbor(i)}} \frac{2h_{ik}^3}{3\mu d_{ik}}(P_i - P_k) + \beta v_{ik}^* d_{ik} + \Phi_i = 0 \tag{8}$$

where h_{ik} and d_{ik} are the current width and length of channel ik respectively, v_{ik}^* the speed of the (flat) solid-liquid interface in this channel, P_i and P_k the pressures at node i and k, and Φ_i a boundary contribution term (i.e., imposed flux condition on node i if it is located at the boundary of the tessellation domain). This resumes the KPL model to solving a matrix problem with standard linear algebra methods (e.g., Gauss elimination).

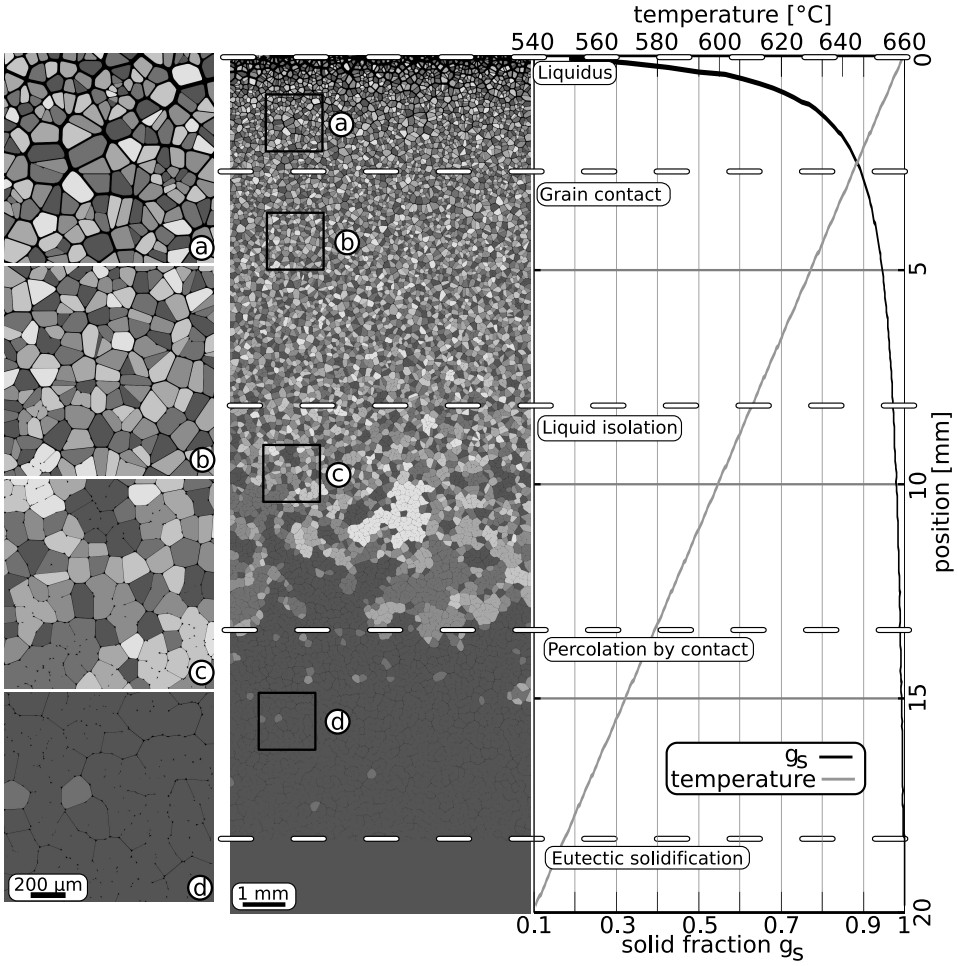

Figure 4: Calculated mushy zone for an Al-1wt%Cu alloy cooled down at -1 K/s in a gradient of 6000 K/m. In order to emphasize the formation of grain clusters, grains in mechanical contact are shaded with the same grey level.

Note that, although the problem is 1D in each channel, the final matrix which multiplies the unknown pressure vector is not tridiagonal as a result of the multiple connectivity of the nodes. Finally, for the smooth grain model, the permeability of the liquid channels is approximated by that of an equivalent rectangle.

3 Localisation phenomena during solidification

3.1 Formation of grain clusters

Figure 4 shows the type of result that can be obtained under steady conditions for the directional solidification of an Al-1wt%Cu alloy. The thermal conditions of this Bridgman-type solidification are a vertical thermal gradient of 60 K/cm and a velocity of $1.6 \cdot 10^{-2}$ cm/s (i.e., cooling rate of -1 K/s). The average grain density was fixed to 10^8 m^{-2}, i.e., average grain size of 100 μm (14 000 grains in the present simulation). The conditions are therefore similar to those reported in [13], but the results have now been obtained with the smooth interface model. Furthermore, different transitions of the mushy zone

are now identified (see below). Otherwise, the features are essentially the same and are only briefly summarised.

The temperature profile is shown on the right of Fig. 4 together with the average solid fraction profile, g_s, computed in horizontal sections of the grain structure shown at the center. The liquid is shown in black and the grains with various grey shades. As the grains are much smaller than the extent of the mushy zone (100 μm compared to more than 1 cm), 4 enlargements of the grain structure are shown on the left with the corresponding scale for typical regions of the mushy zone that are further discussed hereafter. The location of these zones in the grain structure is indicated with black rectangles.

In this low-concentration alloy, g_s rapidly increases just below the liquidus and accordingly the liquid channels are already fairly narrow in the first enlargement (Fig. 4(a)). Their width is mainly a function of the distance between the associated nucleation centers: the closer the nuclei, the thinner the width of the liquid channel. As solidification proceeds, smaller channels get closed while larger ones remain open. Note that the coalescence undercooling at the final stage of solidification is not accounted for in this picture in order to emphasise the mechanical contact between the grains. This phenomenon leads to the formation of grains *clusters*, i.e., a cluster being defined as a group of solid grains which are in mechanical contact. In Fig. 4, the grains belonging to the same cluster are shaded with the same grey level.

The 4 zooms in Fig. 4 characterize well the evolution of the cluster morphology in the mushy zone: in (a) (typically for $0 < g_s < 0.89$), most of the grains are isolated; in (b) ($0.89 < g_s < 0.97$), clusters of a few grains are formed; in (c) ($0.97 < g_s < 0.99$), larger clusters are visible, with a few isolated liquid films remaining inside; in (d) ($0.99 < g_s < 1$), the solid network is continuous and continuous liquid films in the mush no longer exist. These different stages are further analysed in this section. But note already that cluster formation is directly induced by the stochastic nature of the nucleation center location, a feature that has not been considered in past simulation works related to hot tearing.

In order to quantify the clustering or aggregation of grains, it is interesting to compute the specific solid-liquid surface (in 2D length), S_s, i.e., the surface of the solid-liquid interface, S_{sl}, divided by the volume (surface in 2D) of the domain, V_{tot}. This quantity can be normalised by the characteristic length scale of the microstructure d:

$$S_s^\circ = \frac{S_{sl} d}{V_{tot}} \tag{9}$$

Figure 5 shows the computed normalised specific surface, S_s°, as a function of g_s, for a small isothermal volume of an Al-1wt%Cu alloy cooled down at -1 K/s. The + and the $\times$ correspond to the random network of smooth and edgy grains, respectively. These two curves are compared with the regular square and hexagonal arrangements of edgy grains, the lowest normalised specific surface occurring for the hexagonal network (analytical expressions given in Fig. 5). As can be seen, S_s° for these regular arrangements raises monotically with the solid fraction until $g_s = 1$ where it falls abruptly to 0. For

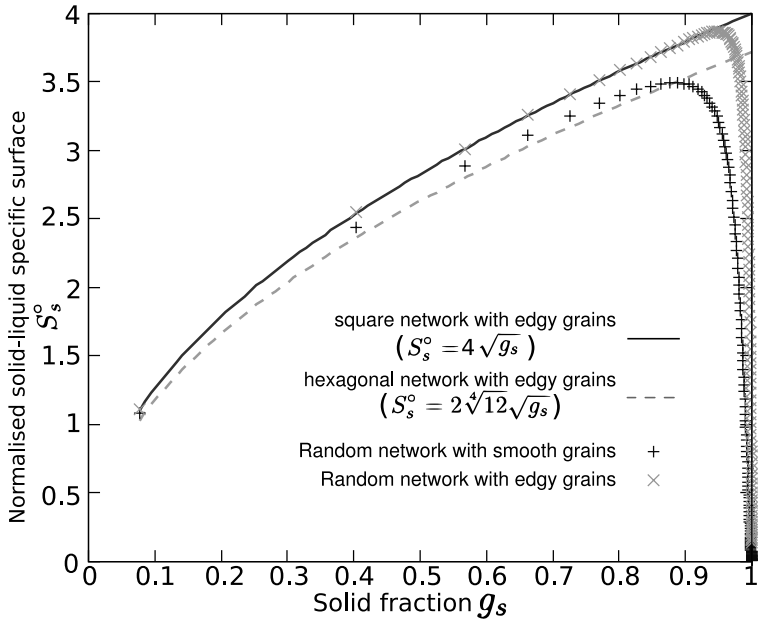

Figure 5: Normalised specific solid-liquid interfacial area,S_s°, as a function of the volume fraction of solid. The theoretical curves calculated for the hexagonal and square network are also shown.

the random numerical models, S_s° has a maximum and smoothly falls to 0, even for the edgy grains. This maximum is reached when the natural increase of solid-liquid interface with grain size is compensated by the progressive closure of liquid channels, i.e., this maximum reveals the formation of an increasing number of clusters. As the grains are slightly rounded in the smooth grain model, they come into contact earlier ($g_s = 0.89$) as compared with the edgy grain model ($g_s = 0.92$ for the edgy grain model). The value of g_s corresponding to the maximum of S_s° will be denoted $g_{s,maxS}$, and corresponds to a number of contacts between grains that is sufficient to overcome the increase of the solid-liquid surface during solidification. It has been marked with a dashed white line in Fig. 4 and is referred to as *grain contact*.

3.2 Localisation of feeding

In order to study the permeability of the mushy zone, an isothermal volume element of the mushy zone is considered at various instants (or values of g_s). Neglecting solidification shrinkage and imposing a pressure difference between the left and right vertical sides of the domain while the top and bottom boundaries are closed, the Poiseuille flow is computed for a volume element containing typically 50×50 grains (size 5×5 mm^2). This numerical experiment allows to view the mush as a homogeneous porous medium and to compute its global permeability.

Figure 6 shows the computed permeability K normalised by the square of the intrinsic specific surface S_v, which is the specific surface (length in 2D) of the solid-liquid interfaces per unit volume of solid V_s, i.e., $S_v = \frac{S_s}{g_s}$. The Carman-Kozeny relationship which relates

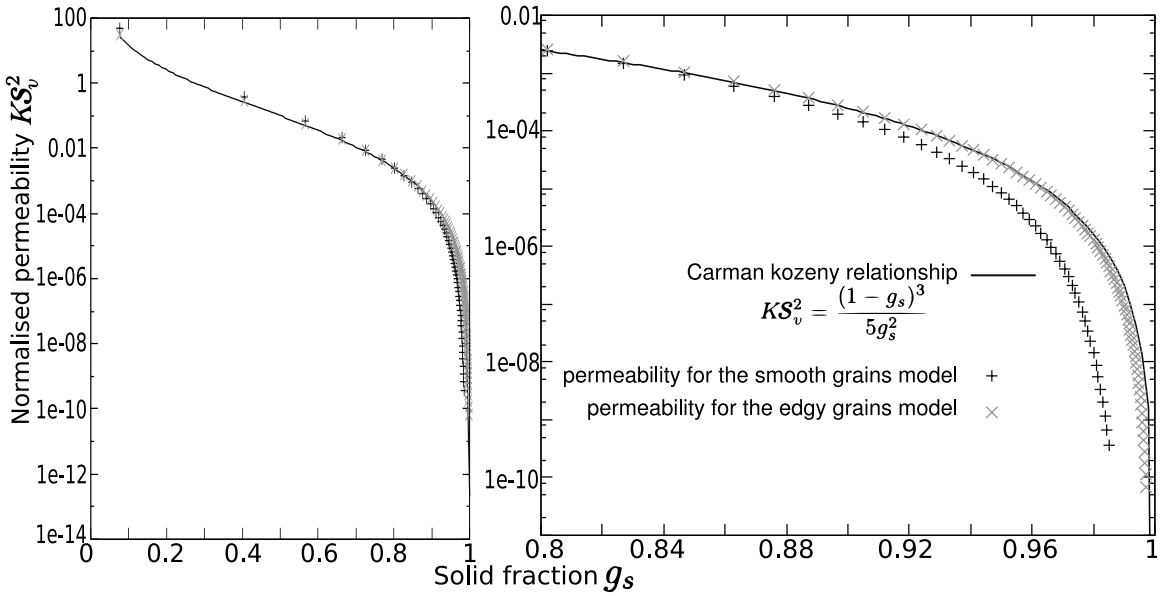

Figure 6: Permeability, K, normalised with the square of the intrinsic specific solid-liquid interface, S_v, as calculated for a random network of grains with the KPL model, assuming edgy or smooth grains. The Carman-Kozeny relationship is also represented for comparison.

the normalised permeability of a packed bed to the solid fraction is also displayed. Note that the general form of this equation is derived from a theoretical network of pipes, while the factor 5 is empirical but shows good agreement with most grain arrangement [21]. As can be seen, the permeability calculated with both KPL models, for smooth and edgy grains (but without losses!), follow the Carman-Kozeny relationship fairly accurately up to very high solid fraction. But for $g_s > 0.92(0.98)$ with the smooth (edgy) grain model, the calculated permeability becomes significantly lower than the prediction of Carman-Kozeny. Whereas, for a regular hexagonal network of grains, it was found that the calculated permeability follows Carman-Kozenys relationship until the very end of solidification [13]. This can be explained by two factors:

- First of all, at high g_s, a few liquid channels are still present but no longer participate to feeding, whereas in a regular arrangement of grains, all the channels remain connected and liquid until $g_s = 1$. In this respect, the smooth grain model leaves isolated liquid pockets at triple junctions and thus induces a departure from Carman-Kozeny earlier as compared with the edgy grain model. This situation is actually closer to observations on organic or metallic alloys, which reveal liquid droplets in between grains (or dendrites)[1]. Despite the fact that these liquid droplets have a positive curvature, the effect of which is not taken into account with the present model, the smooth grain model is nevertheless a much better approximation and will be used exclusively hereafter. It should still be kept in mind that this model overestimates the volume fraction of solid at which flow becomes localised, as it is still 2D and neglects any liquid encapsulated within the grains due

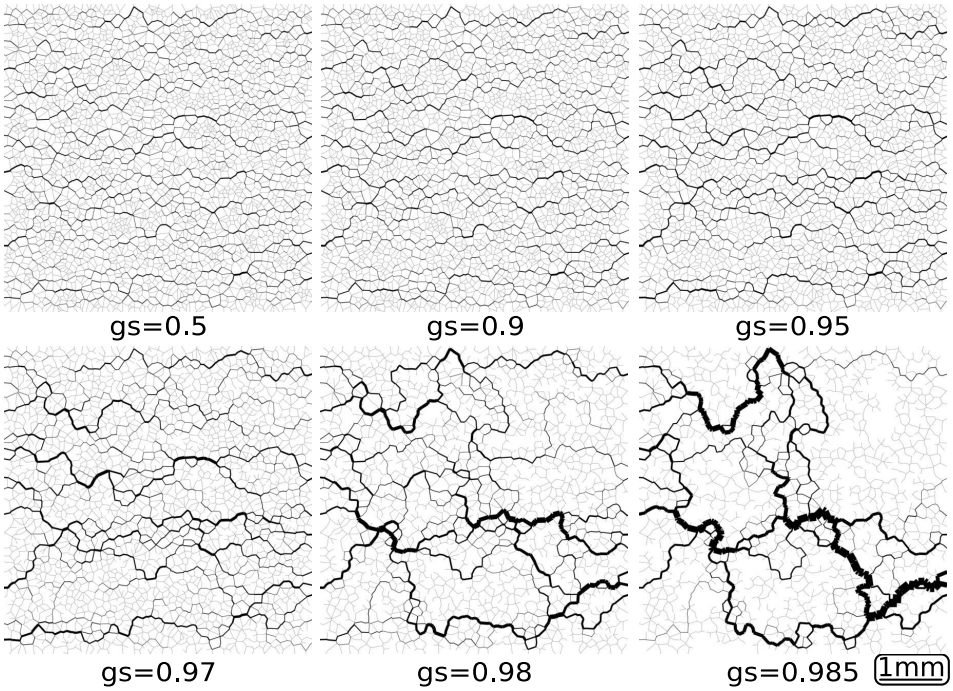

Figure 7: Fluid flow through an isothermal mushy zone volume element (5×5 mm^2), the width of each channel being proportional to the local flow normalised by the overall flow.

to a destabilisation of the interfaces (i.e., globular-dendritic grains).

- The second reason of departure from Carman-Kozenys relationship can be found in Fig. 7. In this figure, the intergranular flow calculated with the KPL smooth grain model is represented with a line, the thickness of which is proportional to the local flow and normalized by the overall flow (i.e., relative flow intensity). At low g_s, the intergranular flow is fairly well distributed among the different channels. When $g_s > 0.97$, the flow tends to be localized along preferential paths. For $g_s = 0.98$, the flow only goes through a few preferential paths while most open liquid channels, despite the fact they are still connected to the continuous channel network, carry a negligible part of the flux (thin grey channels). Note that the characteristic length scale of feeding (for $g_s = 0.98$, typically 1 mm) is substantially larger than the characteristic size of the clusters (for $g_s = 0.98$, the average cluster size is typically 300 μm). Such finding is in agreement with the prediction of the percolation theory [22, 23].

Figure 8 is another illustration of feeding localisation at high volume fraction of solid. It shows a mushy zone of an Al-1wt%Cu alloy with $g_s = 0.98$, the liquid flow in this case being associated with solidification shrinkage. The flow is imposed nil on the right side of the domain, while a nil pressure is imposed on the left side (the top and bottom edges are again closed). The grey scale in this case represents the pressure in the liquid phase. Although the pressure is defined only in the liquid channels, the grey scale is also represented within the grains for visibility. White areas correspond to liquid channels

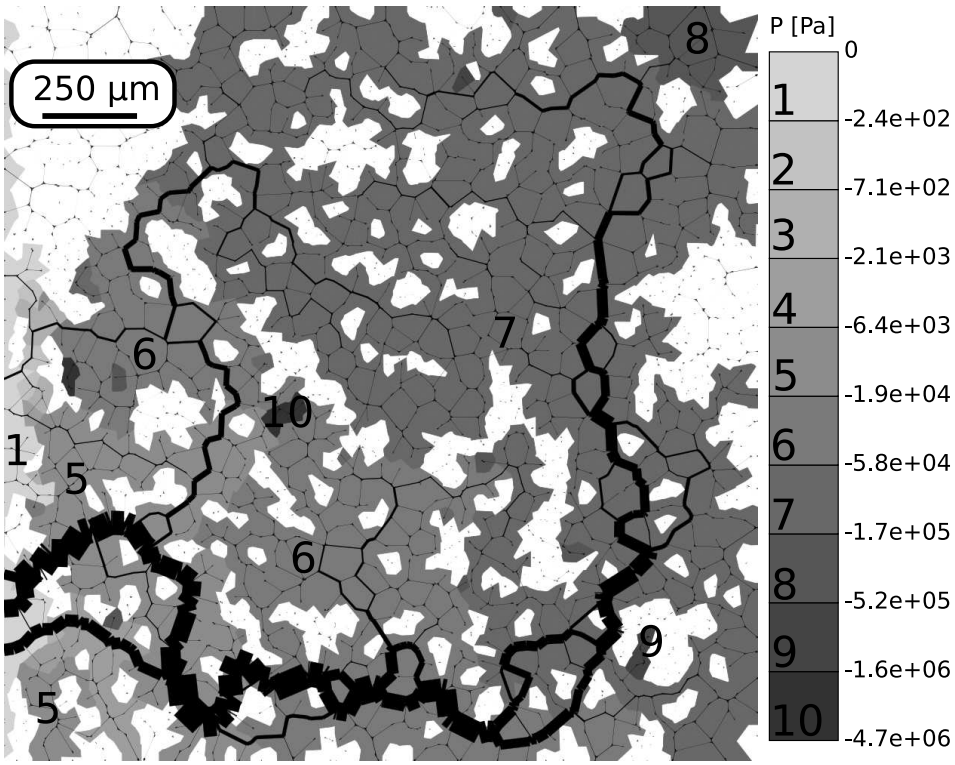

Figure 8: Pressure profile and fluid flow induced by solidification shrinkage for a 2×2 mm^2 mushy zone element. In this sample $T = 590$°C and $g_s = 0.984$. The width of each channel is magnified proportionally to the local flow and its local pressure is indicated with a grey scale (drawn also within the adjacent grains).

which are no longer connected to the main liquid pocket on the left and in which the pressure calculation is no longer performed. The width of the liquid channels has been magnified again proportionally to the local flow.

It appears that there is mainly one path that feeds the entire mush. As a result, a large pressure drop occurs along the main feeding path, typically from 0 kPa at the entrance to -170 kPa near region 7. It is clear that, in real cases, such large pressure drops should be released by the formation of pores/hot cracks. A few channels (white areas) are no longer fed while huge negative pressures (MPa) can be observed in some liquid channels (regions 9 or 10). Such high depression, associated with the hypothesis of fixed and rigid grains, will clearly compete with solid grain deformation/displacement when mechanical aspects will be built in the model.

The feeding ability of a mush can be divided into two steps. At low volume fraction of solid, the mush is well described with a Carman-Kozeny law with the grain size as a typical length scale. At higher value of g_s. it is described by the percolation theory, i.e., with a characteristic length scale which increases with the solid fraction. At this stage, the treatment of the mush as a continuum is not straightforward as feeding is extremely localised. The transition between these two regimes is linked with the appearance of isolated liquid channels, i.e., open liquid channels that are not connected to the feeding

network anymore. This *interdendritic separation*, a term widely used in the literature to describe this occurrence [2, 24], is of course ideal for the initiation of hot tears [3, 5]. In the present contribution, we also argue that liquid feeding is fairly localised at this stage.

From these simulations, the volume fraction of solid, $g_{s,1\%ilc}$, at which 1% of the liquid channels become isolated from the feeding network is computed and called *liquid isolation*. For an Al-1wt%Cu cooled down at -1 K/s, $g_{s,1\%ilc} = 0.97$ (see the corresponding white dashed line drawn in Fig. 4).

3.3 Percolation of solid grains

By definition, a cluster is fully surrounded by a liquid film. As solidification proceeds, the size of the clusters increases until a unique cluster spreads over the whole domain. Note that, in 2D, only one phase can be continuous, either the solid or the liquid, whereas both can be continuous in 3D. In a volume element of uniform temperature such as that shown in Fig. 8, the continuity of the liquid path from the left to the right side can be tested. When there is no longer a liquid path, the solid phase has percolated. In the present case, two criteria can be selected to detect this percolation: 1) the grains can be in "mechanical contact but still separated by nanometric liquid films; 2) the grains are coalesced and the interfaces are dry. These two percolation criteria are called *percolation by contact* and *percolation by coalescence* or *percolation by bridging*, respectively. The corresponding values of g_s are labelled $g_{s,pct}$ and $g_{s,pbr}$, respectively. In the first case, a continuous liquid film still exists but does not allow feeding anymore. It could induce brittle fracture along a still wet path. In the second case, the mechanical behaviour of the mush should be very close to that of the fully (ductile) solid material as only a few discontinuous liquid channels remain. In our model, for an Al-1wt%Cu cooled down at -1 K/s, $g_{s,pct} = 0.985$, a value which is in good agreement with that introduced in the literature [3, 5]. It is also drawn with a dashed white line in Fig. 4 and corresponds visually to the formation of a continuous cluster. Note that the line of percolation by coalescence is not reported in this figure as it occurs fairly below the eutectic solidification.

Figure 9 shows the structure of the clusters for the same mushy zone according to the two percolation criteria. It is clear that clusters formed of truly coalesced grains are always much smaller than clusters of grains which are simply in mechanical contact (with still a nanometric liquid layer). On the second column of Fig. 9, a single cluster spawns in the mush according to the mechanical contact criterion, while a relative fine cluster structure remains according to the bridged interface criterion. Such a situation raises the question of the influence of eutectic solidification on the definitive bridging of the solid, especially in nanometric liquid layers.

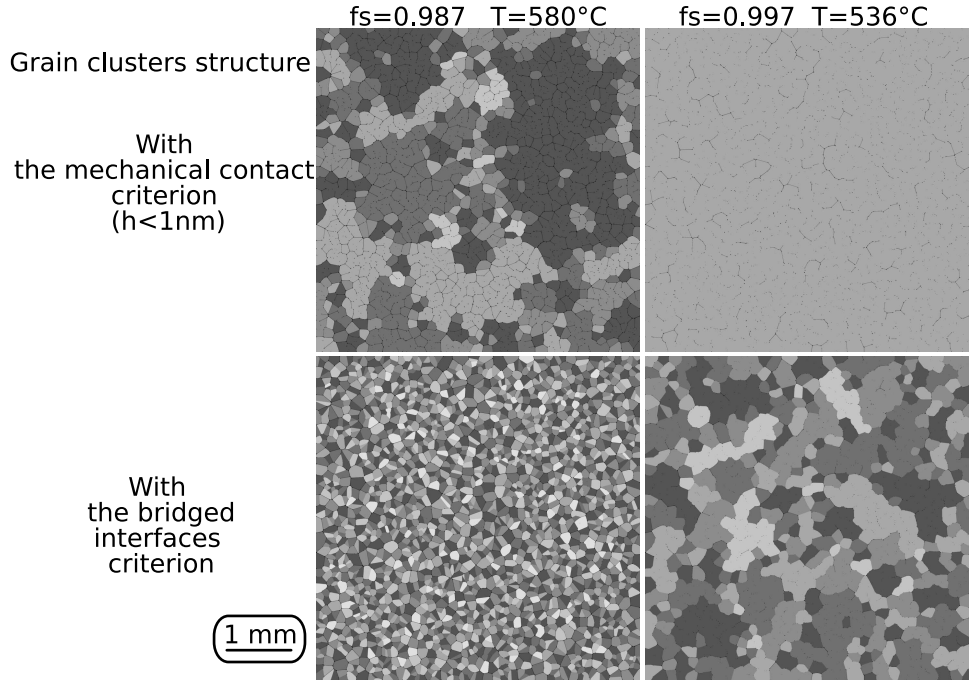

Figure 9: Grain clusters structure for two different criteria, *mechanical contact* and *coalesced/bridged interfaces*.

4 Morphological maps for the mushy zone

Four transitions have been identified in the previous section: 1) $g_{s,maxS}$ (grain contact), when the grain contacts overcome the increase of the solid-liquid interface; 2) $g_{s,1\%ilc}$ when 1% of the liquid channels are isolated from the feeding network; 3) $g_{s,pct}$ when percolation of the solid grains is achieved by simple contact between them (with the possibility of having nanometric liquid films in between); and 4) $g_{s,pbr}$ when the solid grains are percolated via truly coalesced/bridged boundaries.

The first two characteristic values of g_s do not correspond to percolation transitions, just to some states of the mushy zone, but the two last ones are. At $g_{s,pct}$ or $g_{s,pbr}$, the morphology of the mushy zone switches from a continuous liquid path to a continuous cluster. As nucleation is random and the volume element is of finite size, the corresponding solid fractions, $g_{s,pct}$ or $g_{s,pbr}$, might depend on the precise positions of the nuclei. Yet, the equivalence between such a continuum percolation and a lattice percolation have been widely studied [25, 26] and finite size percolation theory states that the standard error for the percolation threshold (i.e., apparition of a continuous cluster) varies according to a power law of the domain (sample) size [22] :

$$\sqrt{< (g_{s,c} - < g_{s,c} >)^2 >} \sim D^{-\frac{1}{\nu}} \tag{10}$$

The average labelled $< . >$ is performed over a large number of simulations done for a given domain of size, D, with various random nuclei configurations. Each of these simulations will give a slightly different value of $g_{s,c}$, the threshold value at which percolation

occurs (in our case, formation of one big cluster by contact or by bridging).$< g_{s,c} >$ is the percolation threshold for an infinite system which is evaluated by an average over a very large number of calculations. Thus, the left hand term of Eq. 10 is the mean deviation of the threshold values. The coefficient ν is the correlation length exponent, function only of the dimensionality of the percolation phenomena: in 2D, this coefficient is equal to 4/3 [22].

In order to check this tendency, simulations have been carried out for an isothermal square domain containing from 100 to 102400 grains. For each domain size, 100 simulations were performed with different repartitions of the nuclei. The computations were done for an Al-1wt%Cu allow cooled at -1K/s. Figure 10 shows the computed solid fraction and temperature at which the 4 transitions are observed as a function of the domain size. Each symbol corresponds to one computation. As can be seen, small domains give a wide spread of the percolation thresholds, while for large domains, the results of the computations are almost superimposed. Nevertheless, the scattered values for small domains are well centred around the mean value. For the two percolation criteria, the domain dependence (Eq. 10) is well verified: the exponent $1/\nu$ is found to be 0.71 ± 0.015 for the percolation by contact and of 0.73 ± 0.04 for the percolation by bridging.

Although the grain contact and liquid isolation values, $g_{s,maxS}$ and $g_{1\%ilc}$, do not correspond to percolation phenomena, they have also been reported in Fig. 10. They converge to well defined values when the size D of the domain increases. For grain contact, a coefficient close to the correlation length exponent is found ($1/\nu = 0.704 \pm 0.001$) whereas for liquid isolation, this coefficient is closer to unity ($1/\nu = 1.11 \pm 0.04$). For this last exponent the discrepancy with the percolation exponent value might be due to the influence of the domain boundary on the liquid isolation criterion (i.e., a liquid film channel touching the border becomes isolated as soon as the two neighbouring channels are closed, whereas, for a liquid film channel within the domain, with four first neighbours in average, there are much more possible paths that can keep it connected to the main liquid network).

Although limited to 2D, this study brings already two valuable informations: First, it enables to determine a critical threshold value of g_s according to a given criterion for an infinite system; Second, for a finite volume of a real mushy zone, e.g., in a thermal gradient, it allows to assess the dispersion of this critical threshold value due to the specific configuration. Such dispersion is especially important for the occurrence of hot tears, which is often difficult to reproduce even under well controlled conditions.

These 4 calculated transitions are reported in the Al-Cu phase diagram as a function of two parameters: the cooling rate, $\dot{T}$, and the solid-liquid interfacial energy, γ_{sl} (Fig. 11). For a fixed density of grains, the first parameter controls essentially microsegregation and thus the temperature at which the first grain contacts are established. More precisely, microsegregation is controlled via the Fourier number, Fo:

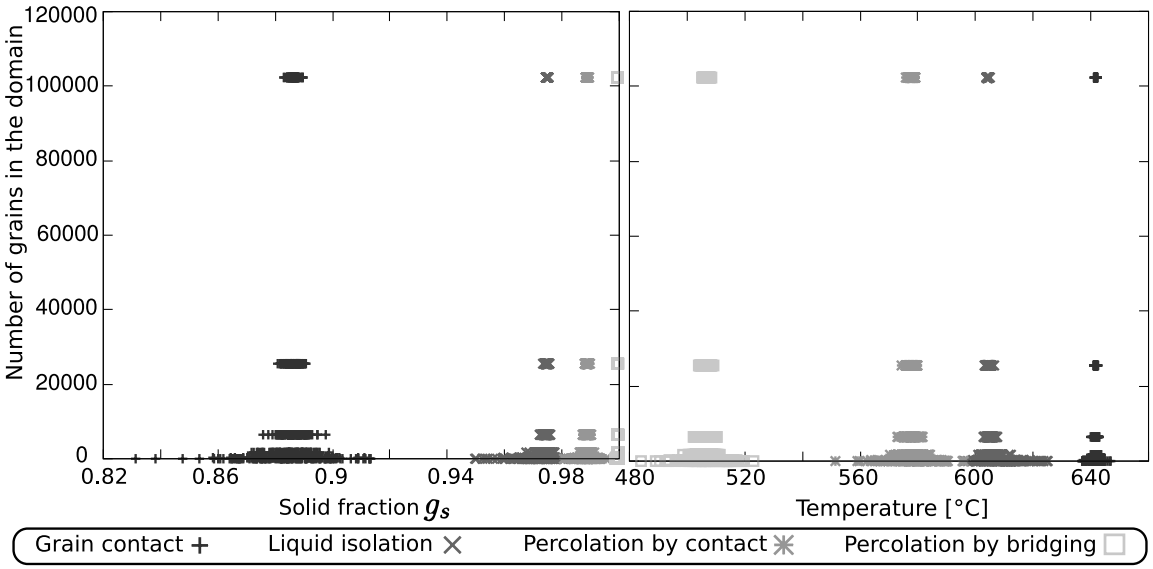

Figure 10: Different transitions of the mushy zone (horizontal axis) as a function of the domain size (vertical axis) according to the following criteria: grain contact (+), $g_{s,maxS}$, liquid isolation (×), $g_{s,1\%ilc}$, percolation by contact (✳), $g_{s,pct}$, and by bridging (□), $g_{s,pbr}$. For each domain size, 100 calculations were carried out with various repartitions of the nuclei.

$$Fo = \frac{D_s \Delta T_0}{d^2 |\dot{T}|} \tag{11}$$

where d is the average grain radius, ΔT_0 the equilibrium solidification interval and D_s is the diffusion coefficient in the solid. Although the Fourier number influences the actual solid fractions at which the various transitions occur[1], its main influence is through the $T(g_s)$ relationship itself: for a fixed value of g_s characterising a given transition of the mushy zone, a fast cooling rate (low Fo) tends to give a relationship $g_s(T)$ close to Scheil-Gulliver (i.e., lower value of $T(g_s)$), whereas a slow cooling rate (high Fo) makes it closer to lever rule. Moreover, the cooling rate influences a second dimensionless number:

$$C = \frac{1}{d} \left(\frac{D_l \Gamma_{sl}}{|\dot{T}|} \right)^{1/3} \tag{12}$$

which corresponds to the ratio of the average radius of curvature at grain corners over the average grain size d (see Eq. 1). A fast cooling rate (small C number) lead to edgy grains, with a low amount of residual liquid ,i.e., contact between grains occurs at higher solid fraction. Within the present model, the solidification is only function of the two previous numbers and the partition coefficient k [19].

The second parameter γ_{sl} is influencing the final stage of coalescence [10]: as repulsive grain boundaries, i.e., boundaries which are characterised by a large coalescence under-

[1]In particular, no geometrical length arises at the two limits of Scheil-Gulliver ($Fo = 0$) and of lever rule ($Fo = \infty$), i.e, all the liquid channels become closed at the same time when $g_s = 1$, and thus no gradual transition occurs within the mushy zone.

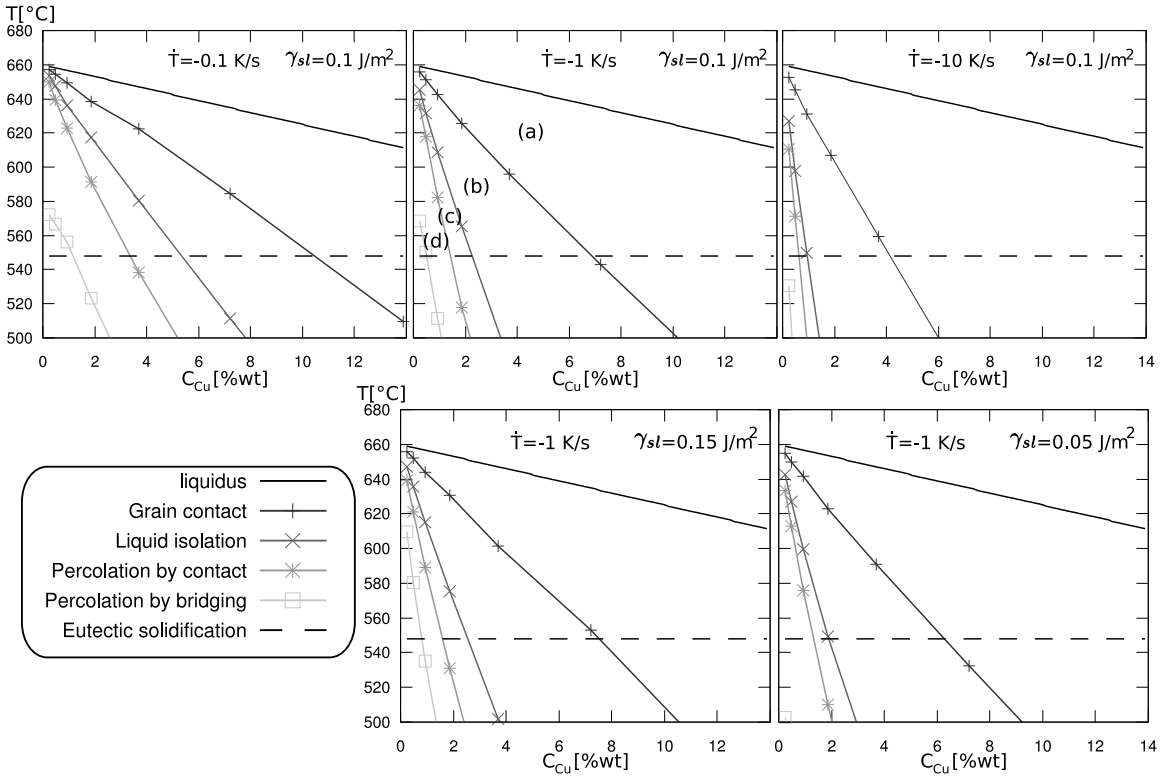

Figure 11: Morphological maps of the mushy zone for different values of the cooling rate, $\dot{T}$, and of the solid liquid surface energy, γ_{sl}. The domains labelled with the letters a-d correspond to the four grain structures in Fig. 4.

cooling, are given by $\gamma_{gb} > 2\gamma_{sl}$, lowering the value of γ_{sl} tends to increase the number of repulsive grain boundaries, i.e., to delay the formation of percolation by bridging.

At the same time, decreasing the solid-liquid interfacial energy has a tendency to make the grains more edgy via its influence on the number C, and thus increase the volume fraction of solid at which the transitions will occur.

These trends are shown in Fig. 11 where the 4 transitions calculated with the granular model have been reported for various concentrations of Cu, keeping the same conditions as those of Fig 4. Note that the solidus has not been reported on the maps as it is meaningless, mainly due to microsegregation. As described above, an increased cooling rate makes the transition lines steeper. A decrease of the interface energy significantly shifts down the transition line associated with percolation by bridging and slightly shifts down the other transitions lines.

As expected, for very low solute content, a fully coalesced solid appears quickly, before eutectic solidification. Moreover, for a large nominal concentration in Cu (more than 8 wt% Cu), eutectic solidification occurs before contact between the grains. In the concentration range where the hot tearing sensitivity increases (0.5-3 wt% Cu), most of the solidification time is spent between liquid isolation and percolation by contact, where localisation phenomena are intense. For nominal concentrations where the hot cracking sensitivity decreases (> 3 wt% Cu), solidification time is spent between grain contact and liquid isolation. Note that, in a way, this finding is similar to the Clyne-Davis hot tearing

criterion [3], but in the present model no a priori parameters are required.

These transitions might help in understanding the main deformation mechanism of the material at high temperature, in relation with hot tearing. Between the liquidus and the point of grain contact (i.e., $0 < g_s < g_{s,maxS}$), grains moves freely in the mush and liquid feeding is easy (figure 4 (a)). Between grain contact and liquid isolation (i.e., $g_{s,maxS} < g_s < g_{s,1\%ilc}$), the permeability of the mush decreases drastically and the formation of clusters starts to localise deformation (figure 4 (b)). Between liquid isolation and percolation by contact (i.e., $g_{s,1\%ilc} < g_s < g_{s,pct}$), feeding is almost impossible and very localised. Moreover, large clusters are present; this localises deformation induced by thermal contraction and solidification shrinkage at the cluster boundaries (figure 4 (c)). This region of the mushy zone is therefore very brittle. Between percolation by contact and percolation by coalescence (i.e., $g_{s,pct} < g_s < g_{s,pbr}$), the mechanical properties of the mush are very close to the fully solid material. Deformation of the mushy zone will be more ductile, but at some remaining liquid films, opening is still possible, with probably plastic deformation of the already established solid bridged (figure 4 (d)). Once the material has reached the line of percolation by coalescence, its mechanical properties are very close to the fully solid material.

5 Conclusion

Although based on fairly simplified assumptions, this granular model offers several interesting features for equiaxed grains. First, it shows the progressive formation of grains clusters. This phenomenon is important considering that grain clusters should localise deformation on their edges, especially thermal contraction. Second, the model allows to calculate liquid feeding and its localization at high volume fraction of solid. Third, it enables to compute the percolation of grain clusters, i.e., the formation of a continuous solid phase.

As transitions between different stages of solidification can be numerically estimated, maps showing the morphology of the mushy zone for any parameters can be dawn. Morphology transitions within the mushy zone, which have to be artificially introduced in continuum approaches, appear naturally with the present model. They are important as they define the dominant deformation mechanism of the material.

Finally a full mechanical model considering mechanical coupling between solid and liquid phases is now under development by the present authors. This approach should give more quantitative results on the determinant phenomena for hot cracking. Moreover, as the model is not heavy in computation time, an extension to 3D is feasible, thus providing interesting opportunities for the modelling of hot tearing under realistic conditions.

6 Acknowledgement

This research is funded by Alcan CRV (France) and ANRT (Association Nationale de la Recherche Technique, France) . The authors would like to thank Prof. J. Dantzig from UIUC (USA), V. Mathier from LSMX EPFL (Switzerland) and B. Commet from Alcan-CRV (France) for fruitful discussions.

References

[1] I. Farup, J.M. Drezet, and M. Rappaz. In situ observation of hot tearing formation in succinonitrile-acetone. *Acta Mater.*, 49:1261–69, 2001.

[2] J.C. Borland. Generalised theory of super-solidus cracking in welds. *Brit. Weld. J.*, 7:508, 1960.

[3] T.W. Clyne and G.J. Davies. The influence of composition on solidification cracking suceptibility in binary alloy systems. *J. Brit. Foundry*, 74:65–73, 1981.

[4] U. Feurer. *Giesserei Forsch*, 2:75–80, 1976.

[5] M. Rappaz, J. Drezet, and M. Gremaud. A new hot-tearing criterion. *Met. Mater. Trans.*, 30A:449–55, 1999.

[6] Braccini M. *Optimisation des pièces moulées : Étude des phénomènes de fissuration à chaud dans les alliages Al-Cu.* PhD thesis, INPG, 2000.

[7] O. Ludwig, J.M. Drezet, Ch. Martin, and M. Suéry. Rheological behavior of Al-Cu alloys during solidification. *Met. Mater. Trans.*, 36A:1525–35, 2005.

[8] M. M'Hamdi, A. Mo, and Ch. Martin. Two-phase modeling directed toward hot tearing formation in aluminium direct chill casting. *Met. Mater. Trans.*, 33A:2081–93, 2002.

[9] V. Mathier, J.M. Drezet, and M. Rappaz. Two-phase modeling of hot tearing in aluminum alloys using a semi-coupled method. In *Modeling of Casting, Welding and Advanced Solidification Processes.* (TMS Publ., Warrendale, USA), 2006.

[10] M. Rappaz, A. Jacot, and W. Boettinger. Last stage solidification of alloys : Theorical model of dendrite arm and grain coalescence. *Met. Mater. Trans.*, 34A:467–479, 2003.

[11] A.H. Dahle and D.H StJohn. Rheological behavior of the mushy zone and its effect on the formation of casting defects during solidification. *Acta Mater.*, 47(1):31–41, 1999.

[12] V. Mathier, A. Jacot, and M. Rappaz. Coalescence of Equiaxed Grains During Solidification. *Mod. Sim. Mat. Sci. Eng.*, 12:479–490, 2004.

[13] S. Vernède and M. Rappaz. Transition of the Mushy Zone from Continuous Liquid Films to a Coherent Solid. *Phil. Mag.*, 86(23):3779–94, 2006.

[14] D.J. Lahaie and M. Bouchard. Physical modeling of the deformation mechanism of semisolid bodies and a mechanical criterion for hot tearing. *Met. Mater. Trans. B*, 32B:697–705, 2001.

[15] W. O. Dijkstra, C. Vuik, A. J. Dammers, and L. Katgermann. In *Solidification Processes and Microstructures.* M. Rappaz, Ch.Beckermann, R. Trivedi, (TMS Publ., Warrendale, PA, USA), 2004.

[16] Ch. Charbon and M. Rappaz. Shape of grain boundaries during phase transformations. *Acta Mater.*, 44:2663–68, 1996.

[17] C.B. Barber, D.P. Dobkin, and H.T. Huhdanpaa. The quickhull algorithm for convex hulls. *ACM Trans. of Mathematical Software*, 22:469–83, 1996.

[18] I. Ohnaka. Mathematical analysis of solute redistribution during solidification with diffusion in solid phase. *Trans. ISIJ*, 26:1045, 1986.

[19] S. Vernède and M. Rappaz. A simple and efficient model for mesoscale solidification simulation. *submited to Acta Mater.*, 2006.

[20] A. Jacot and M. Rappaz. A pseudo-front tracking technique for the modelling of solidification microstructures in multi-component alloys. *Acta Mater.*, 50:1909–26, 2002.

[21] P.C. Carman. Fluid flow through granular beds. *Trans. Inst. Chem.*, 15:150, 1935.

[22] D. Stauffer and A. Aharony. *Introduction to percolation theory.* Taylor and Francis, 1994.

[23] B. I. Halperin, S. Feng, and P.N. Sen. Differences between lattice and continuum percolation transport exponents. *Phys. Rev. Lett.*, 54(22):2391–94, 1985.

[24] D.G. Eskin, Suyitno, and L. Katgerman. *Prog. Mat. Scie.*, 49:629–711, 2004.

[25] A. R. Kerstein. Equivalence of the void percolation problem for overlapping spheres and a network problem. *J. Phys. A*, 16:3071–3075, 1983.

[26] W. T. Elam, A.R. Kerstein, and J.J. Rehr. Critical properties of the void percolation problem for spheres. *Phys Rev Lett.*, 52(17):1516, 1984.